



Forschungszentrum Karlsruhe
in der Helmholtz-Gemeinschaft

Wissenschaftliche Berichte
FZKA 6933

Stress Intensity Factors and T-stress for Volume Strains in Crack Surface Layers

T. Fett, G. Rizzi

Institut für Materialforschung

Dezember 2003

FORSCHUNGSZENTRUM KARLSRUHE

in der Helmholtz-Gemeinschaft

Wissenschaftliche Berichte

FZKA 6933

**STRESS INTENSITY FACTORS AND
T-STRESS FOR VOLUME STRAINS IN
CRACK SURFACE LAYERS**

T. Fett, G. Rizzi

Institut für Materialforschung

Forschungszentrum Karlsruhe GmbH, Karlsruhe

2003

Impressum der Print-Ausgabe:

**Als Manuskript gedruckt
Für diesen Bericht behalten wir uns alle Rechte vor**

**Forschungszentrum Karlsruhe GmbH
Postfach 3640, 76021 Karlsruhe**

**Mitglied der Hermann von Helmholtz-Gemeinschaft
Deutscher Forschungszentren (HGF)**

ISSN 0947-8620

Stress intensity factors and T-stress for volume strains in crack surface layers

Abstract:

In brittle materials, e.g. ceramics and glass, thin zones at the crack surfaces are affected by volume strains caused by different effects. In zirconia ceramics a transformation zone with compressive stresses develops around crack tips due to a stress-induced tetragonal-to-monoclinic phase transformation. In piezoelectric ceramics domains may switch in stress direction and switch back when exposed to a changed stress state near the free crack faces during crack growth. In the case of glass, strains may be generated in the presence of water by a volume change due to ion exchange effects. For all problems mentioned above it is sufficient to know the effects behind the crack tip.

This report provides the fracture mechanics parameters that enable a theoretical treatment of such transformation zones. First, Green's functions for small zone elements are derived. Then, mode-I and mode-II stress intensity factors as well as T-stress solutions are determined for zones of constant height and zones with a square-root-shaped profile.

Spannungsintensitätsfaktoren und T-Spannung für Volumendehnungen in der Nähe von Rissflanken

Kurzfassung:

In spröden Materialien wird der Bereich der Rissflanken durch Volumendehnungen beeinflusst. Mehrere Effekte sind für diese Dehnungen verantwortlich. In Zirkonkeramiken entwickelt sich aufgrund der martensitischen Umwandlung im singulären Risspitzen-Spannungsfeld eine Phasentransformationszone. Bei Rissfortschritt gelangt diese Zone in den Bereich der Rissflanken. Bei Piezokeramiken verursacht das Risspitzen-Spannungsfeld eine Umschaltung der Domänen in die Hauptspannungsrichtung. Im Falle von Gläsern kann es bei Anwesenheit von Wasser im Riss zum Ionenaustausch und damit einer Volumenabnahme kommen. Alle Effekte führen zu Spannungen und damit zu einer Belastung des Risses.

Ziel des Berichts ist die Ermittlung von Mode-I- und Mode-II-Spannungsintensitätsfaktoren sowie der T-Spannung unter derartiger Belastung. Neben der Herleitung der entsprechenden Greens-Funktionen werden für spezielle Zonenprofile die K-Faktoren und T-Spannungen angegeben.

Contents

1. Introduction	1
2. Green's functions for stress intensity factors and T-stress	3
2.1 Basic procedure	3
2.2 Mode-I stress intensity factor	4
2.3 Mode-II stress intensity factor	7
2.4 T-stress	9
3. X-stresses inside the zones	12
4. Practical applications	15
4.1 Layer ending at the crack tip ($s_0=0$)	15
4.1.1 Mode-I stress intensity factor	15
4.1.2 Mode-II stress intensity factor	17
4.1.3 T-stress	17
4.2 Layer ending at some distance from the crack tip ($s_0>0$)	18
4.3 Superposition of solutions	19
4.4 Strains varying with crack tip distance	20
References	21

1. Introduction

Weight function techniques for stress intensity factors and T-stresses are widely applied in fracture mechanics to tractions distributed along a crack at the distance $y=0$, i.e. along the crack faces (Fig. 1). These tractions may be a real crack-face pressure or fictitious stresses occurring in the uncracked component at the location of a crack exposed to a crack face loading by the principle of superposition.

In many cases, local strains occur near the crack surfaces (in general, for $y \neq 0$). An example is shown in Fig. 1 where the region behind the crack tip is affected only.

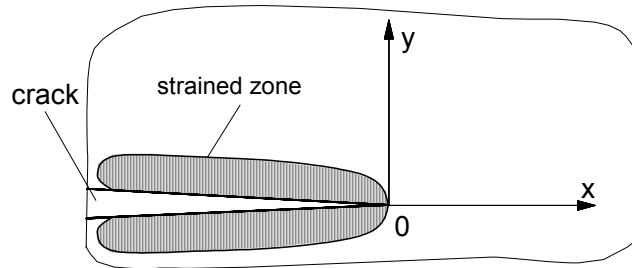


Fig. 1 Crack with a crack face zone exposed to volumetric strains.

Some effects responsible for such strains shall be listed here:

- Stabilized zirconia ceramics may undergo a stress-induced tetragonal-to-monoclinic phase transformation. As a result, a transformation zone with compressive stresses develops around the crack tips, leading to an increase in fracture toughness. The increase in fracture toughness depends on the size of the transformation zone. Whereas the cordially-shaped initial transformation zone yields a disappearing shielding stress intensity factor (Fig. 2a), a finite shielding stress intensity factor is generated by a growing crack [1-3]. These phase transformations that are now located in the wake of the growing crack are mainly responsible for an increase in the crack resistance curve (R-curve) factor.
- In piezoelectric ceramics (PZT) domains located in the neighbourhood of the crack tip stress field may switch to the direction of maximum principal stress. In the case of a growing crack, part of these reoriented domains may switch back when they “feel” the changed stress state near the free crack faces. Although the domain switching effects occur under constant volume, computation of shielding stress intensity factors is very similar to that of phase transformations, where a volume change is responsible for the shielding stress intensity factor [4-7].
- Strains may also be generated in the crack surface region by a volume reduction or expansion due to diffusion effects. In the special case of glass, there is experimental evidence [8-11] of a thin hydration layer developing at the crack surfaces during selective alkali leaching via ion exchange. Generation of surface tensile stresses has

been attributed to a volume contraction associated with a repolymerisation of silanol groups that are left in the near-surface region of the glass.

For all problems mentioned above it is sufficient to know the effects behind the crack tip (Fig. 2b). In order to simplify the geometry, the crack wake zones are chosen to end at a straight line through the crack tip. It is the aim of this report to provide mode-I and mode-II stress intensity factors as well as T-stress solutions for strains in this region.

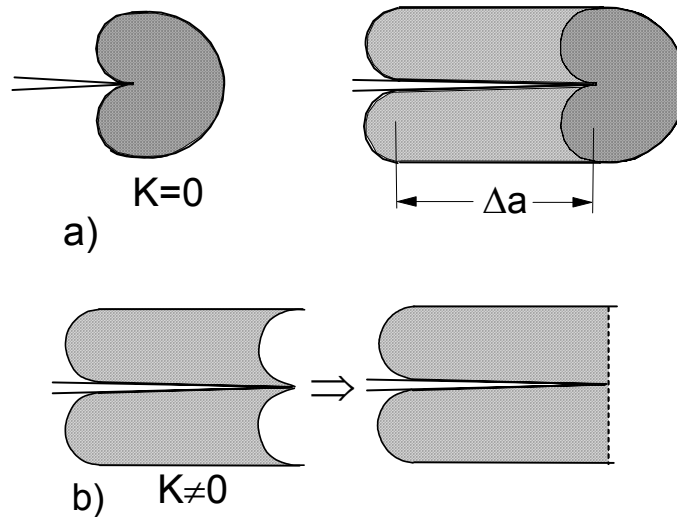


Fig. 2 a) Left: Initial transformation zone of a ceramic undergoing a stress-induced tetragonal-to-monoclinic phase transformation, right: extension of this zone during crack growth by Δa , b) left: zone part responsible for the generation of a finite shielding stress intensity factor, right: approximation of the zone by a straight cut-off at the crack tip.

2. Green's functions for stress intensity factors and T-stress

2.1 Basic procedure

The principal treatment of located strain region problems may be explained by a zone of constant thickness b along the crack wake. For this case, the procedure developed by McMeeking and Evans [1] is illustrated in Fig. 3. The layer of height $2b$ is (Fig. 3a) is assumed to be subjected to a volumetric strain ϵ^c . Since free contraction is prevented by the bulk material, tensile stresses for contractive strain ($\epsilon^c < 0$) and compressive stresses for expansive strains ($\epsilon^c > 0$) must occur. These stresses are responsible for a stress intensity factor contribution ΔK that can be computed by using an Eshelby technique ([1, 12]), in Fig. 3 applied to positive strains.

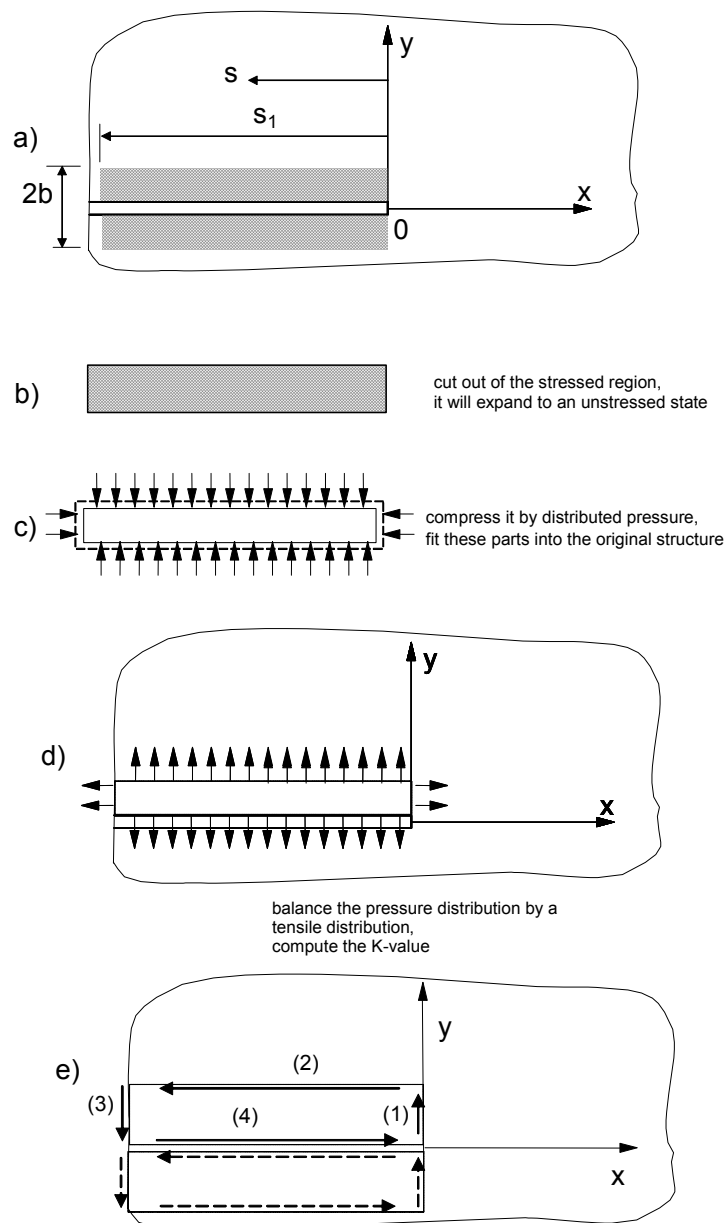


Fig. 3 Computation of the stress intensity factor.

Let us assume the crack face layer to be removed from the original material (Fig. 3b). Under unconstrained conditions, the material exhibits a volumetric strain ε^e and is assumed return to its original shape by applying surface tractions to the contour of the transformation zone (Fig. 3c). The zone now fits into the body again and an equilibrium can be obtained by nullifying the surface tractions with a layer of body forces (Fig. 3d).

The surface tractions are given by the normal pressure p defined by

$$p = \frac{\varepsilon^e E}{3(1-2\nu)}, \quad (1)$$

where E is Young's modulus and ν Poisson's ratio.

2.2 Mode-I stress intensity factor

The stress intensity factor can be computed similar to the R-curve, as was done first by McMeeking and Evans [1]. The mode-I contribution then results as

$$\Delta K_I = p \oint_{\Gamma} \mathbf{n} \cdot \mathbf{h} dS \quad (2)$$

with the normal vector \mathbf{n} on the zone contour. Γ is the contour line of the zone and dS is a line length increment. The contour is illustrated in the upper half of Fig. 3e by the straight lines (1)-(4) and similar lines in the lower half. The vector \mathbf{h} represents the weight function $\mathbf{h}_I = (h_{I,y}, h_{I,x})^T$ with the components $h_{I,y}$ and $h_{I,x}$

$$h_{I,x} = \frac{1}{\sqrt{8\pi r(1-\nu)}} [2\nu - 1 + \sin(\theta/2) \sin(3\theta/2)] \cos(\theta/2) \quad (3a)$$

$$h_{I,y} = \frac{1}{\sqrt{8\pi r(1-\nu)}} [2 - 2\nu - \cos(\theta/2) \cos(3\theta/2)] \sin(\theta/2). \quad (3b)$$

In these relations r and θ are the polar coordinates with the origin at the crack tip. Using the theorem of Gauss, eq.(2) can be rewritten as [1]

$$\Delta K_I = p \int_{(A)} \text{div } \mathbf{h}_I \, dx \, dy \quad (4)$$

and

$$\text{div } \mathbf{h}_I = \frac{\partial h_{I,x}}{\partial x} + \frac{\partial h_{I,y}}{\partial y} \quad (5)$$

where A is the area in the x - y plane (extending above and below the crack plane, Fig. 3e and Fig. 4a, but not necessarily symmetrical). For a numerical evaluation of the stress intensity factor ΔK it may be of advantage to carry out the integration over y from the crack surface to the zone height b . For the case of a zone located symmetrically above and below the crack ($dA = -2b \times dx = 2b \times ds$),

$$d(\Delta K_I) = \frac{\varepsilon^c E}{1-\nu} \sqrt{b} g_I(s/b) d(s/b) \quad (6)$$

with the function g_I (subscript I stands for the mode-I stress intensity factor) defined by

$$g_I = \frac{2(1-\nu)}{3(1-2\nu)} \int_0^1 \left(\frac{\partial h_{I,x}(r/b)}{\partial(x/b)} + \frac{\partial h_{I,y}(r/b)}{\partial(y/b)} \right) d(y/b) \quad (7)$$

It should be noted that g_I is independent of Poisson's ratio, since the pre-factor in (7) cancels ν out. The function $g_I(s/b)$ is shown in Fig. 4a. Its asymptotic behaviour is given by the straight lines described by

$$g_I(s/b) = \begin{cases} -0.25/\sqrt{s/b} & \text{for } s/b \rightarrow 0 \\ -0.1/(s/b)^{5/2} & \text{for } s/b \gg 1 \end{cases} \quad (8)$$

An interpolation of these limit functions for example is given by

$$g_I \approx -\frac{1}{4\sqrt{s/b} + 5(s/b)^{3/2} + 10(s/b)^{5/2}} \quad (9)$$

from which for an arbitrarily varying zone $b(s)$

$$\Delta K_I = \frac{\varepsilon^c E}{1-\nu} \int_0^{s_1} g_I(s'/b') \frac{1}{\sqrt{b'}} d(s') \quad (10)$$

can be derived easily by a single integration.

The following considerations shall refer to the special case of a zone with *constant thickness*. This special case can be treated simply by the direct evaluation of eq.(2). Numerical evaluation of the integral expression yields

$$\Delta K_I = -C_I \frac{\varepsilon^c E}{1-\nu} \sqrt{b} \quad , \quad \varepsilon^c < 0 \quad (11)$$

with the coefficient C_I (subscript I stands for mode-I) represented as circles in Fig. 4b and compiled in Table 1 for some values of s/b . In this context, it should be noted that in [1] a limit value of 0.37 is given, which is in agreement with the present results.

If a zone is considered to extend between the locations s_0 and s_1 (Fig. 5), it holds for $s_0 > 3b$ that

$$\Delta K_I \cong -\frac{\varepsilon^c E}{1-\nu} \sqrt{b} \frac{1}{15} \left(\frac{1}{(s_0/b)^{3/2}} - \frac{1}{(s_1/b)^{3/2}} \right) \quad (12)$$

s/b	C_I	s/b	C_I
0.1	0.1490	7	0.3726
0.3	0.2314	10	0.3740
1	0.3236	20	0.3754
2	0.3543	30	0.3757
3	0.3638	100	0.37606
5	0.3703	∞	0.37613

Table 1 Coefficient C_I of eq.(11).

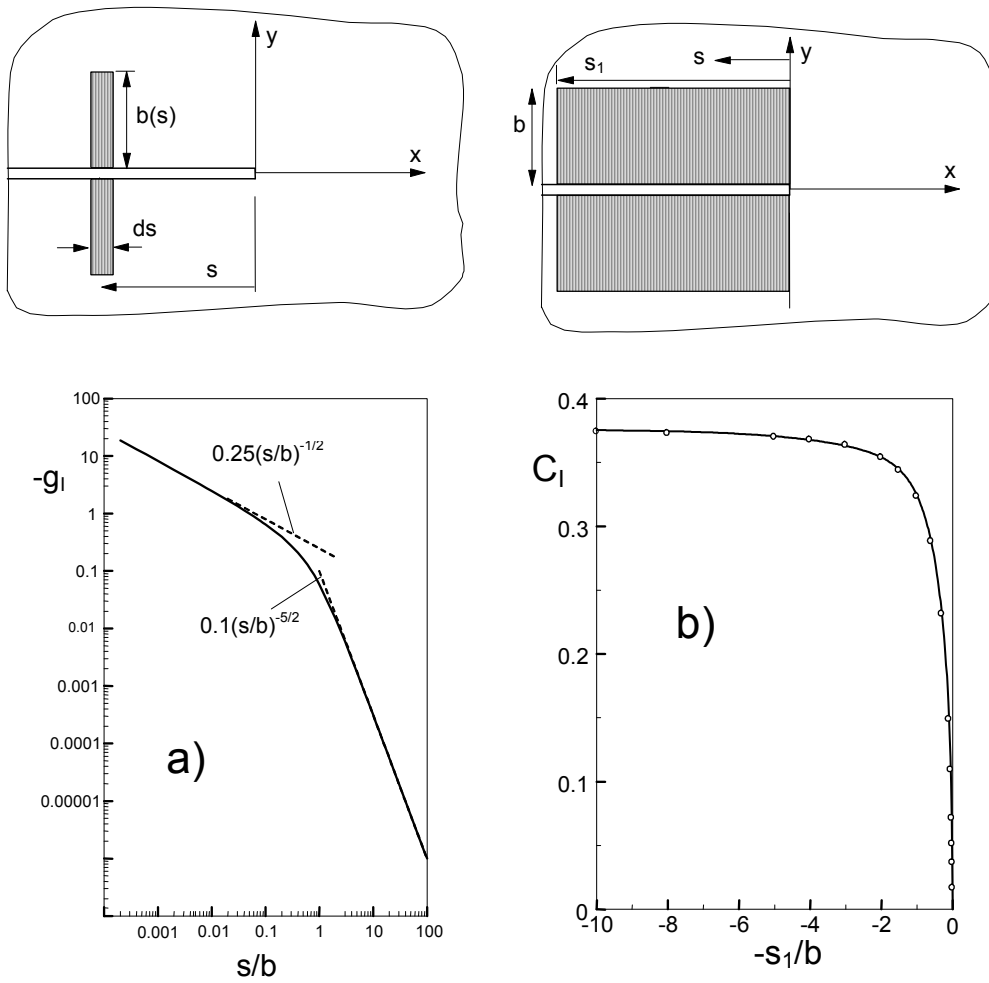


Fig. 4 a) Green's function g_I as stress intensity factor for a strip-shaped zone width, b) stress intensity factor coefficient C_I for a zone of constant height b according to eq.(11).

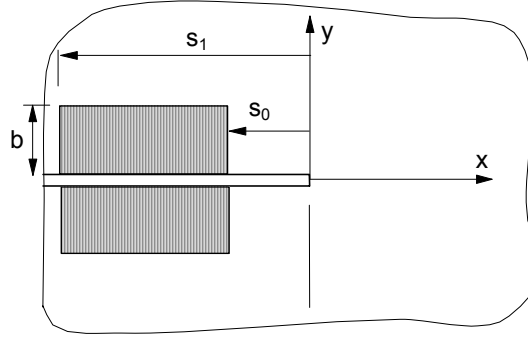


Fig. 5 Finite zone of constant height b .

2.3 Mode-II stress intensity factor

In the case of a volume strain zone which is not developed symmetrically to the crack plane, also a mode-II stress intensity factor must result. The related weight functions h_{II} read

$$h_{II,x} = \frac{1}{\sqrt{32\pi r(1-\nu)}} [4 - 4\nu + \cos(\theta) + \cos(2\theta)] \sin(\theta/2) \quad (13a)$$

$$h_{II,y} = \frac{1}{\sqrt{32\pi r(1-\nu)}} [2 - 4\nu + \cos(\theta) - \cos(2\theta)] \cos(\theta/2) \quad (13b)$$

as derived in the Appendix.

The mode-II stress intensity factor ΔK_{II} for a zone segment of length ds lying on one side of the crack is plotted in Fig. 6, where now g_{II} is defined by

$$g_{II} = \frac{(1-\nu)}{3(1-2\nu)} \int_0^1 \left(\frac{\partial h_{II,x}(r/b)}{\partial(x/b)} + \frac{\partial h_{II,y}(r/b)}{\partial(y/b)} \right) d(y/b) \quad (14a)$$

$$\Delta K_{II} = \frac{\varepsilon^c E}{1-\nu} \int_0^{s_1} g_{II}(s'/b') \frac{1}{\sqrt{b'}} d(s') \quad (14b)$$

The asymptotes of g_{II} (introduced in Fig. 6 as straight lines) are

$$g_{II}(s/b) = \begin{cases} 0.095 & \text{for } s/b \rightarrow 0 \\ \frac{1}{15}(s/b)^{-3/2} & \text{for } s/b \gg 1 \end{cases} \quad (15)$$

where the lower solution for $s/b \gg 1$ yields sufficiently accurate results for $s/b \geq 2$ already. An interpolation for the full s/b range is given by

$$g_{II} \cong \frac{1}{\frac{21}{2} + 15(s/b)^{3/2}} \quad (16)$$

The corresponding mode-I stress intensity factor for this non-symmetric zone is given as one half of the stress intensity factor computed for the symmetric case (see Fig. 4a).

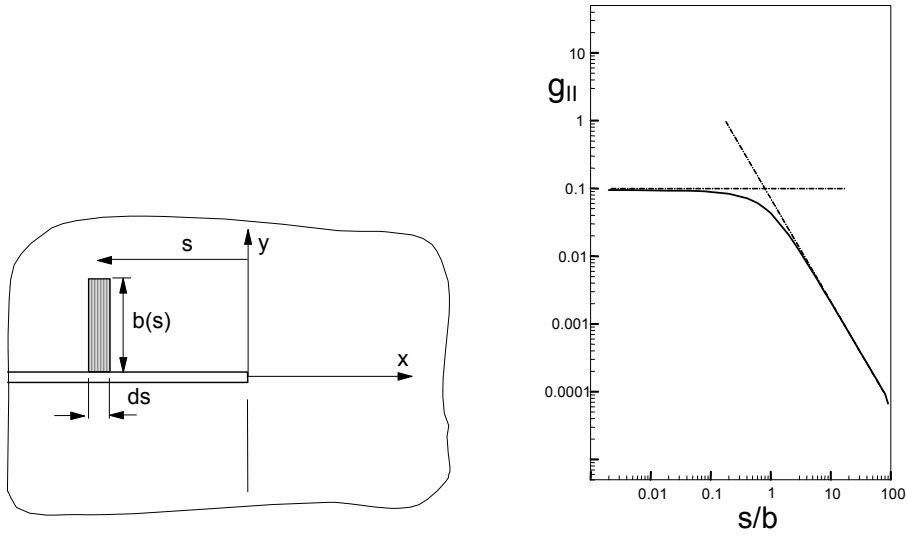


Fig. 6 Mode-II stress intensity factor contribution for a single zone of width ds located on one side of the crack exclusively.

As an example, let us compute the mode-II stress intensity factor K_{II} for the case of a zone of constant height b at the upper side of the crack extending from $s = s_0$ to $s = s_1$ (Fig. 7a). Figure 7b shows the mode-II stress intensity factor expressed by the coefficient C_{II}

$$\Delta K_{II} = C_{II} \frac{\varepsilon^c E}{1-\nu} \sqrt{b} \quad (17a)$$

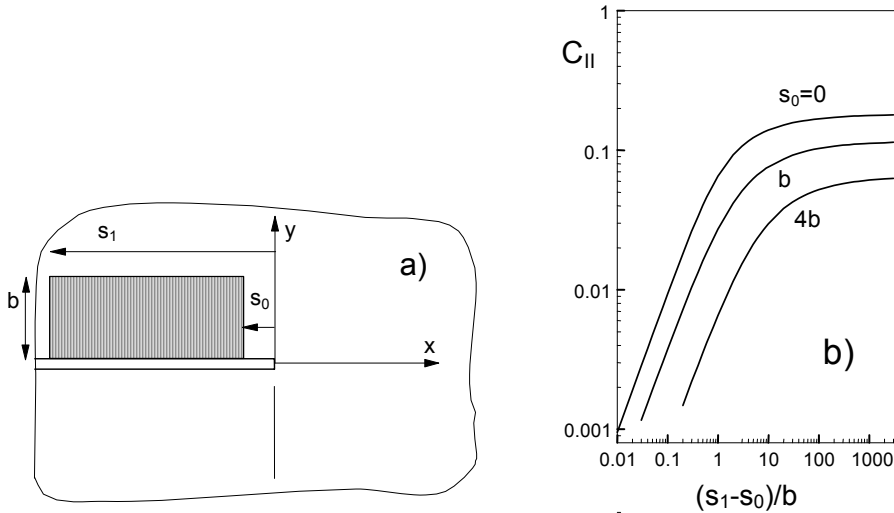


Fig. 7 Mode-II stress intensity factor for a non-symmetric zone.

For $s_0=0$, the coefficient C_{II} reads

$$C_{II} \cong 0.00834 \left\{ \sqrt{3}\pi - 6\sqrt{3} \arctan \left[\frac{1}{\sqrt{3}} \left(1 - 2(10/7)^{1/3} \sqrt{\frac{s_1}{b}} \right) \right] + \right. \\ \left. + 3 \ln 7 + 3 \ln [7 + 7^{1/3} 10^{2/3} \sqrt{s_1/b}] - 6 \ln \left[7 + 7^{2/3} 10^{1/3} \sqrt{\frac{s_1}{b}} \right] \right\} \quad (17b)$$

2.4 T-stress

Two approaches based on the application of the finite element (FE) method were used to determine the T-stress term caused by a contractive surface layer. First, pairs of zone increments with height b and width Δs at distance s from the crack tip were evaluated. Whereas in the analytical evaluations of Sections 2.2 and 2.3, infinitesimally small zone widths ds could be achieved, the finite element method needs a finite zone width Δs . The contractive volumetric strain was obtained by solving a simple thermoelastic problem, namely, thermal expansion by localised temperature change. The temperature inside the zone segment $b \times \Delta s$ was chosen to be $\Theta = -1^\circ$ whereas in the remaining structure zero temperature was prescribed. Poisson's ratio was chosen as $\nu = 0.2$ which is typical of ceramic materials (especially glass). For the material with a thermal expansion coefficient of α_Θ , the volumetric contractive strain is

$$\varepsilon^c = 3\alpha_\Theta \Theta \quad (18)$$

Computations were carried out with ABAQUS Version 6.2 and provided the stress intensity factors K_I as well as the T-stress term. The results obtained for different zone heights b could be represented by a common geometric function $g_{\Delta T}$ in the form of

$$\Delta T = -\frac{\varepsilon^c E}{1-\nu} \frac{1}{b} g_{\Delta T}(s/b) \Delta s \quad (19)$$

where now s is the distance of the *zone centre* from the crack tip. The function $g_{\Delta T}$ is plotted in Fig. 8.

For $s/b \gg 1$, the asymptotic relation

$$g_{\Delta T} = \frac{1}{6} (s/b)^{-2} \quad (20)$$

results. For $s/b \ll 1$, $g_{\Delta T} \cong 1/6$ is obtained. An approximate interpolation relation is then given by

$$g_{\Delta T} \cong \frac{1}{6} \frac{1}{1 + (s/b)^2} \quad (21)$$

The result of Fig. 8 may be used as the Green's function for large s/b at least, where the zone width Δs is sufficiently small compared with the distance s .

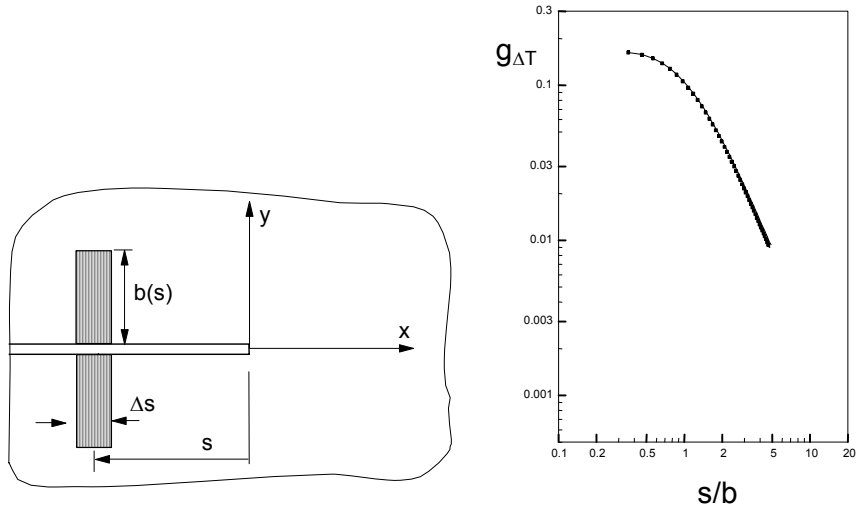


Fig. 8 T-stress for zones of finite width Δs .

A second method results from the use of a monotonously increased zone widths and a constant zone height b . The curve $T(s)$ provides the infinitesimal result $\partial T/\partial s$ by differentiating with respect to the upper limit, i.e.

$$T = \int_{s_0}^{s_1} \frac{\partial T}{\partial s'} ds' \quad (22)$$

The differential quotient $\partial T/\partial s$ then yields the function g_T defined by

$$\frac{\partial T}{\partial s} = \frac{\varepsilon^c E}{1-\nu} \frac{1}{b} g_T(s/b) \quad (23)$$

and, finally,

$$T = -\frac{\varepsilon^c E}{1-\nu} \int_{s_0}^{s_1} g_T(s'/b') \frac{1}{b'} ds' \quad (24)$$

Figure 9a shows the T-stress in a normalised form

$$T^* = -T(s_1) \frac{1-\nu}{\varepsilon^c E} \quad (25)$$

as a function of s for $s_0=0.1b$ and $b=1$. The numerical results for T^* at any s/b in the range of $0.1 < s/b < 5$ were determined by interpolating the data of Fig. 9b using cubic splines. The first derivative with respect to s is plotted in Fig. 9c. From this curve, the same dependency was obtained than for single zone sections, namely,

$$g_T \cong \frac{1}{6} \frac{1}{1+(s/b)^2} \quad (26)$$

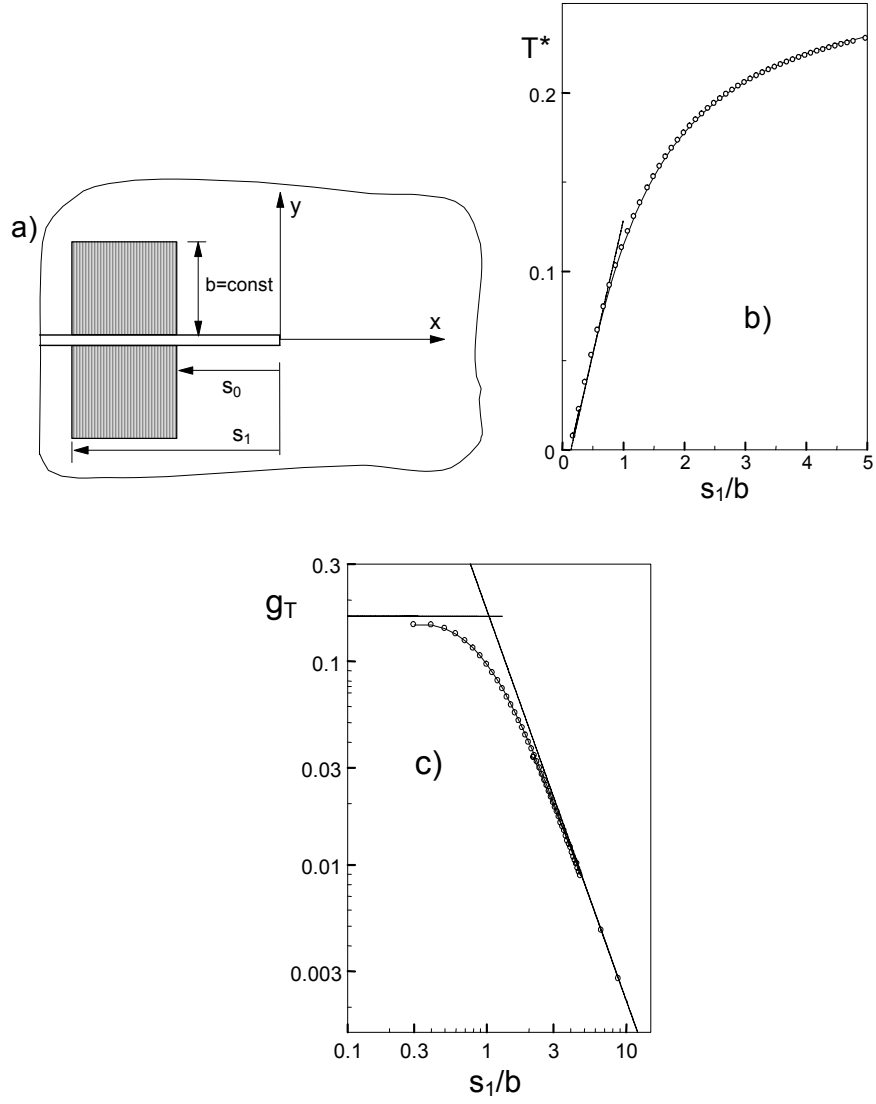


Fig. 9 T-stress for a monotonously increasing layer width s at $s_0=b$.

A layer of constant height b (extending from $s_0>0$) causes the T-stress

$$T \cong -\frac{1}{6} \frac{\varepsilon^c E}{1-\nu} [\arctan(s_1/b) - \arctan(s_0/b)] \quad (27a)$$

as can be obtained by introducing eq.(26) in (24). For the zone extending from $s_0=0$, it holds

$$T \cong -\frac{1}{6} \frac{\varepsilon^c E}{1-\nu} \arctan(s_1/b) \quad (27b)$$

3. X-stresses inside the zones

Stresses in the contractive layer are of interest with respect to the study of diffusion effects. The rate of ion exchange depends on the actual stresses in the zone. Tensile stresses will increase and compressive stresses decrease this rate. In the case of domain switching in piezoelectric ceramics, these stresses may enhance or suppress back switching of domains depending on the sign of the stress. This would influence the crack resistance curve (R-curve), as was outlined in [6,7].

The maximum stress in a thin layer of constant height on a bulk material of the same elastic properties is given by

$$\sigma_{\max} = -\frac{\varepsilon^c E}{3(1-\nu)} = -\frac{\varepsilon_{\text{lin}} E}{1-\nu} \quad (28)$$

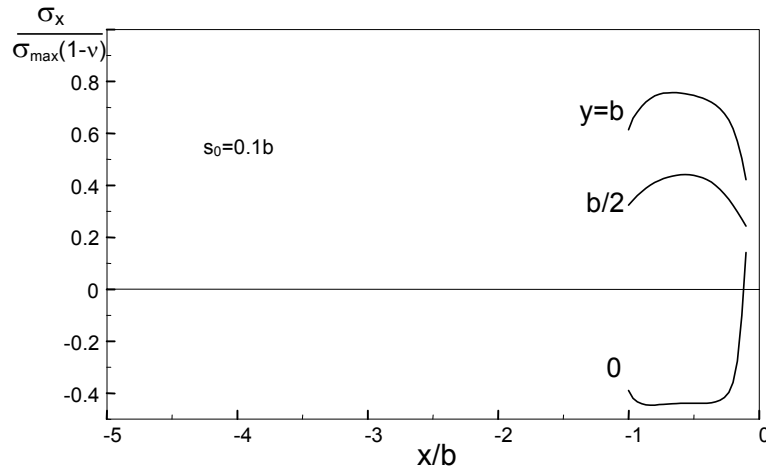
The factor 3 in the denominator reflects the fact that ε^c is the volume strain that is three times the linear strain ε_{lin} . Equation (28) results from the Bernoulli hypothesis for a layer of large lateral dimensions compared to thickness.

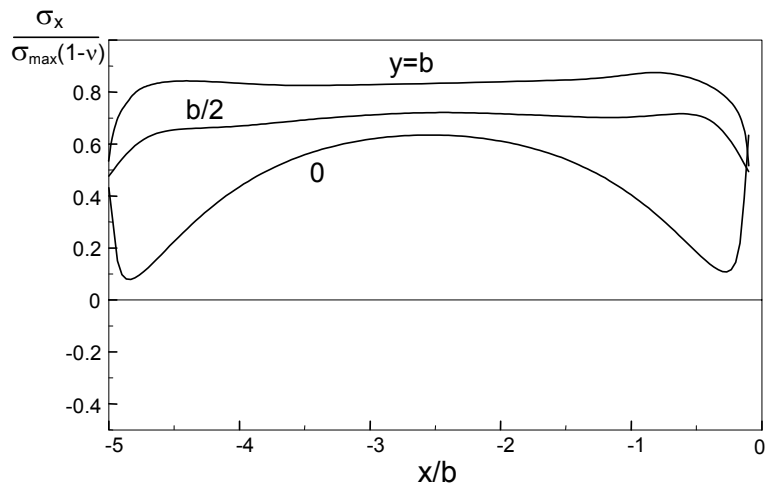
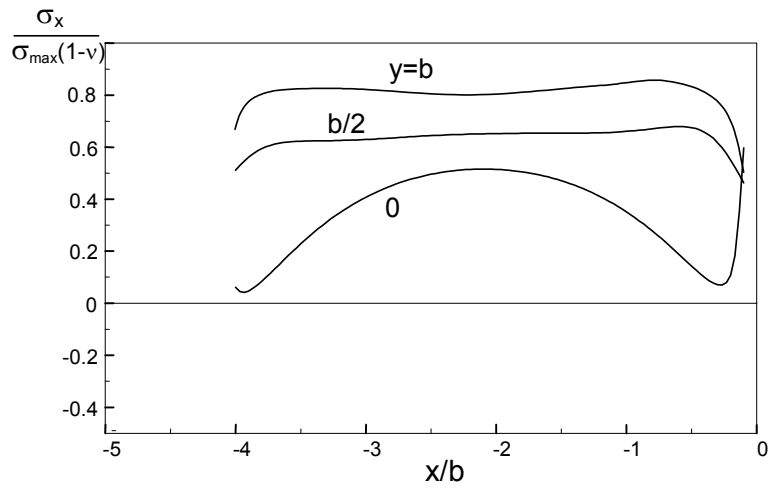
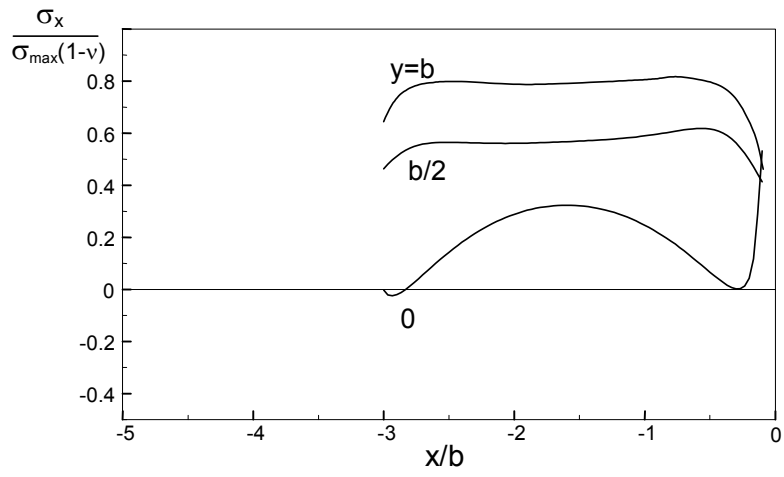
Having in mind that the layer is part of a crack, the σ_x stresses of the crack, consisting of the T-stress and higher-order terms, are superimposed. This gives rise to deviations from eq.(28) which therefore has to be considered a rough estimation.

Figure 10 shows the σ_x -stress component for two zone lengths s_1-s_0 and three depths, namely, $y=0$, $y=b/2$, and $y=b$.

With increasing zone length s_1/b , the x-stress component increases for all three depths and most significantly for the surface $y=0$. The maximum x-stress obtained for $y=b$ reaches about $\sigma_x \approx 0.85(1-\nu)\sigma_{\max}$ for $s_1/b=5$, i.e. $\sigma_x \approx 0.7\sigma_{\max}$. For zones of larger length (see Fig. 10 for $s_1/b=20$), the maximum stresses are reached at a distance of $y=0$ and $y=b/2$ from the surface, i.e.

$$\sigma_x \approx 0.9\sigma_{\max}$$





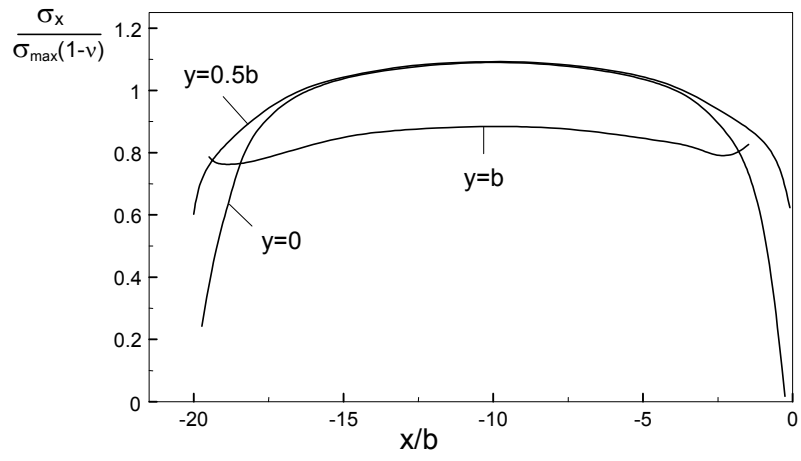


Fig. 10 Stress component σ_x in the contractive layer at variable distances y from the free surface and different zone lengths s_1 and $s_0=0.1b$.

4. Practical applications

In a first computation, the shielding stress intensity factor is determined for a hydration layer at the surface of a crack in glass. The basis are data provided by Michalske et al.[8-10]. From these papers (Fig. 5 in [8]) it can be concluded that for a 30%Na₂O/10%B₂O₃/60%SiO₂ glass in 5mol HCl solution at $da/dt=10^{-7}$ m/s, the hydration layer height is 1.6μm at $s=60$ μm crack tip distance. Zone height is proportional to the square root of time

$$b \propto \sqrt{t} \quad (29)$$

4.1 Layer ending at the crack tip ($s_0=0$)

If the whole crack is assumed to be filled with water, the zone height under a constant crack growth rate ($s \propto t$) becomes [8-10]

$$b = \alpha\sqrt{s} \quad (30)$$

(see Fig. 11a) with $\alpha=0.21\sqrt{\mu\text{m}}$.

4.1.1 Mode-I stress intensity factor

The mode-I stress intensity factor resulting from a hydration layer with an arbitrarily varying zone thickness $b(s)$ is given by eq.(10). Numerical computations were performed by direct application of eq.(7).

In Fig. 11b the stress intensity factors ΔK_I are plotted for this zone profile and different values of the proportionality factor α . For small values of s all curves coincide, exhibiting a slope of $\frac{1}{2}$ in the log-log plot. For large values a saturation is visible. The limit value ΔK_{lim} depends on α , as visible from Fig. 11b and Fig. 11c

$$\Delta K_{\text{lim}} = -\frac{2}{5}\alpha \frac{\varepsilon^c E}{1-\nu} \quad \text{for} \quad \sqrt{s_1} / \alpha \gg 1 \quad (31)$$

Integration of eq.(10) with the approximate Green's function of eq.(9), g_I , from $s=0$ to $s=s_1$ results in

$$\Delta K_I = -\frac{\varepsilon^c E}{1-\nu} \frac{4\alpha}{3\sqrt{15}} \left\{ \arctan \left[\frac{1}{3} \sqrt{\frac{5}{3}} \left(1 + \frac{4}{\alpha} \sqrt{s_1} \right) \right] - \arctan \left[\frac{1}{3} \sqrt{\frac{5}{3}} \right] \right\} \quad (32)$$

i.e.

$$\Delta K_I = -\frac{\varepsilon^c E}{1-\nu} \frac{4\alpha}{3\sqrt{15}} \arctan \left[\frac{\frac{4}{3} \sqrt{\frac{5}{3}} \sqrt{s_1} / \alpha}{1 + \frac{5}{27} (1 + 4\sqrt{s_1} / \alpha)} \right] \quad (33)$$

From this relation, the limit stress intensity factor is obtained as

$$\Delta K_{\text{lim}} = -\alpha \frac{\varepsilon^c E}{1-\nu} \frac{4}{3\sqrt{15}} \arctan \sqrt{27/5} = -0.401 \alpha \frac{\varepsilon^c E}{1-\nu} \quad (34)$$

in good agreement with the numerical evaluation (31).

As shown in Fig. 11b, the limit value is sufficiently approximated by

$$\Delta K_I \geq 0.95 \Delta K_{\text{lim}} \quad \text{for} \quad s_1 / \alpha^2 \geq 85 \quad (35)$$

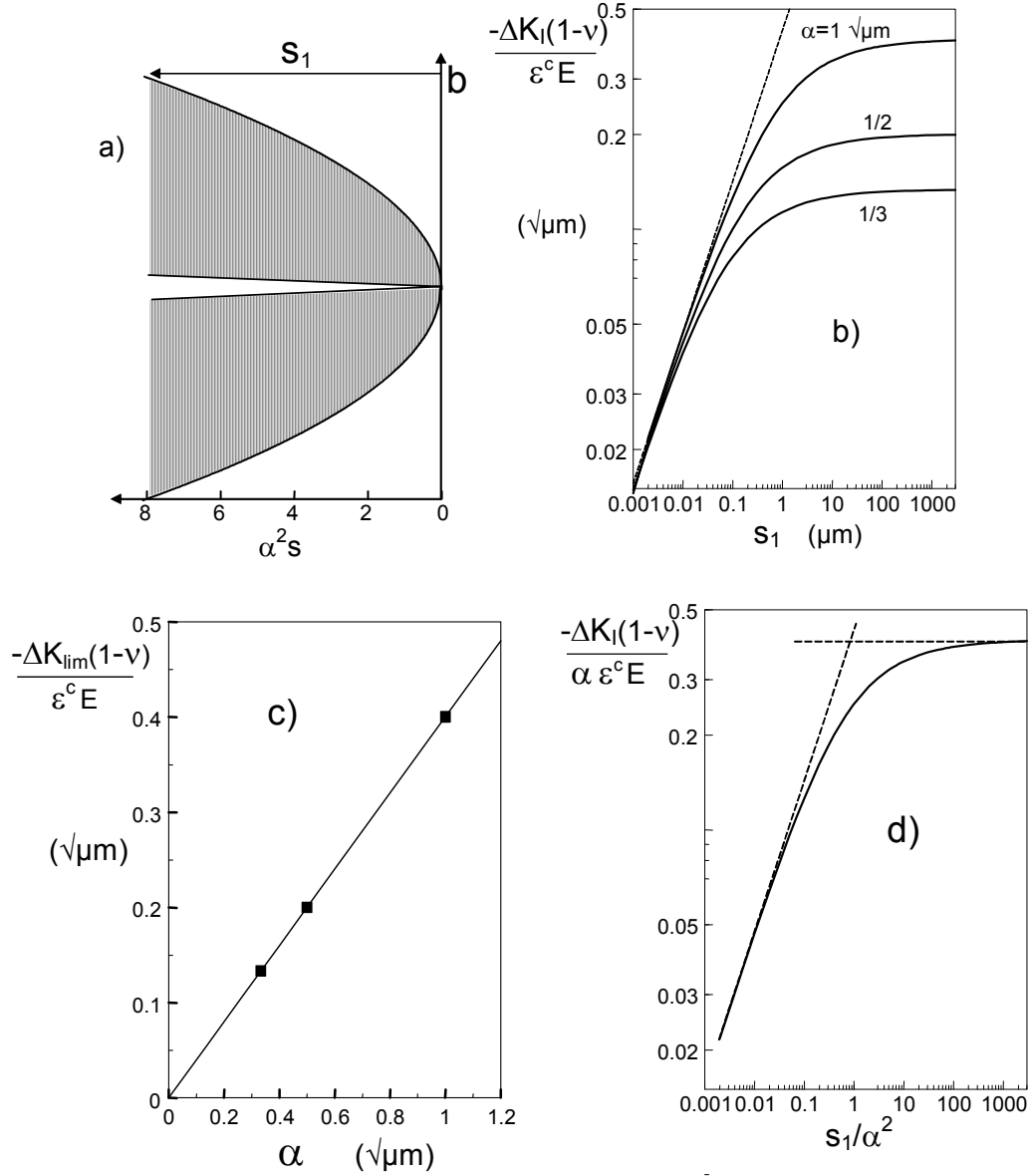


Fig. 11 a) Square-root-shaped zone profile (symmetrical to the crack plane) reaching to the crack tip, b) shielding stress intensity factor ΔK_I as a function of zone length s_1 , c) limit value ΔK_{lim} for varying values of α defined by eq.(30), d) normalised representation of a).

For a simpler use, the asymptotic solutions may be applied, instead of eq.(33), i.e.

$$\Delta K_I = -\frac{\varepsilon^c E}{1-\nu} \times \begin{cases} \frac{1}{2} \sqrt{s_1} & \text{for } s_1 / \alpha^2 \rightarrow 0 \\ \frac{2}{5} \alpha & \text{for } s_1 / \alpha^2 \rightarrow \infty \end{cases} \quad (36)$$

The second limit case represents a sufficient approximation for zones in practical applications.

4.1.2 Mode-II stress intensity factor

For a square-root-shaped zone extending on one crack surface exclusively (Fig. 12a), the mode-II stress intensity factor ΔK_{II} was determined by use of eqs.(14a), (14b), and (30). The result is shown in Fig. 12b. It becomes obvious that in this loading case no saturation value of ΔK_{II} appears. An analytical expression for the mode-II stress intensity factor ΔK_{II} is obtained by evaluation of eq.(14b) with the approximate Green's function (16). It results

$$\Delta K_{II} = \frac{\varepsilon^c E}{1-\nu} \frac{4}{45} \alpha \ln \left(1 + \frac{10 s_1^{3/4}}{7 \alpha^{3/2}} \right) \quad (37)$$

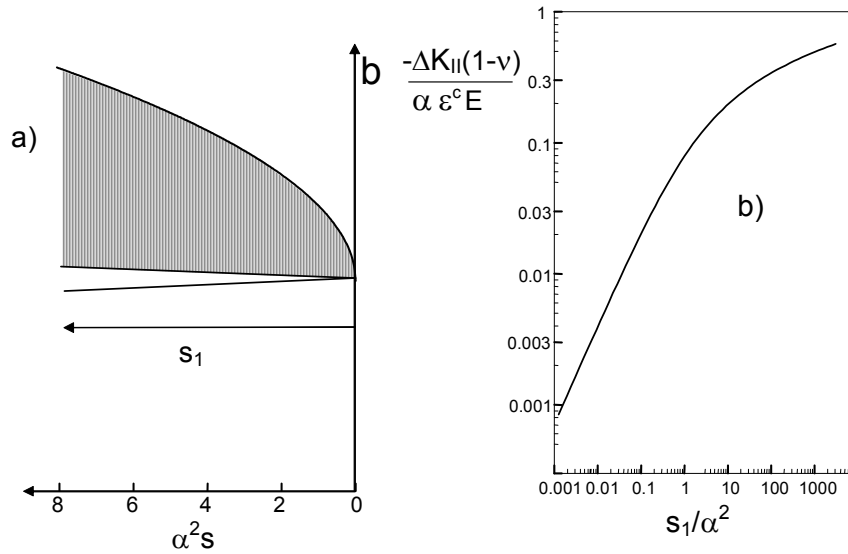


Fig. 12 a) Zone extending on one crack surface, b) mode-II stress intensity factor ΔK_{II}

4.1.3 T-stress

The T-stress related to the symmetric zone shape given by eq.(30) results

$$T = -\frac{1}{3} \frac{\varepsilon^c E}{1-\nu} \arctan(\sqrt{s_1} / \alpha) \quad (38)$$

by evaluation of eqs.(24), (26), and (30).

4.2 Layer ending at distance $s_0 > 0$ from the crack tip

For the case that liquid water cannot reach the crack tip due to the very small crack opening in this region, a zone profile of

$$b = \alpha \sqrt{s - s_0} \quad (39)$$

has to be expected (Fig. 13a), which causes the limit stress intensity factor of

$$\Delta K_{\text{lim}} = -\frac{\varepsilon^c E}{1-\nu} \times \begin{cases} \frac{2}{15} \alpha^2 / s_0 & \text{for } \alpha / \sqrt{s_0} \rightarrow 0 \\ \frac{2}{5} \alpha / \sqrt{s_0} & \text{for } \alpha / \sqrt{s_0} \rightarrow \infty \end{cases} \quad (40)$$

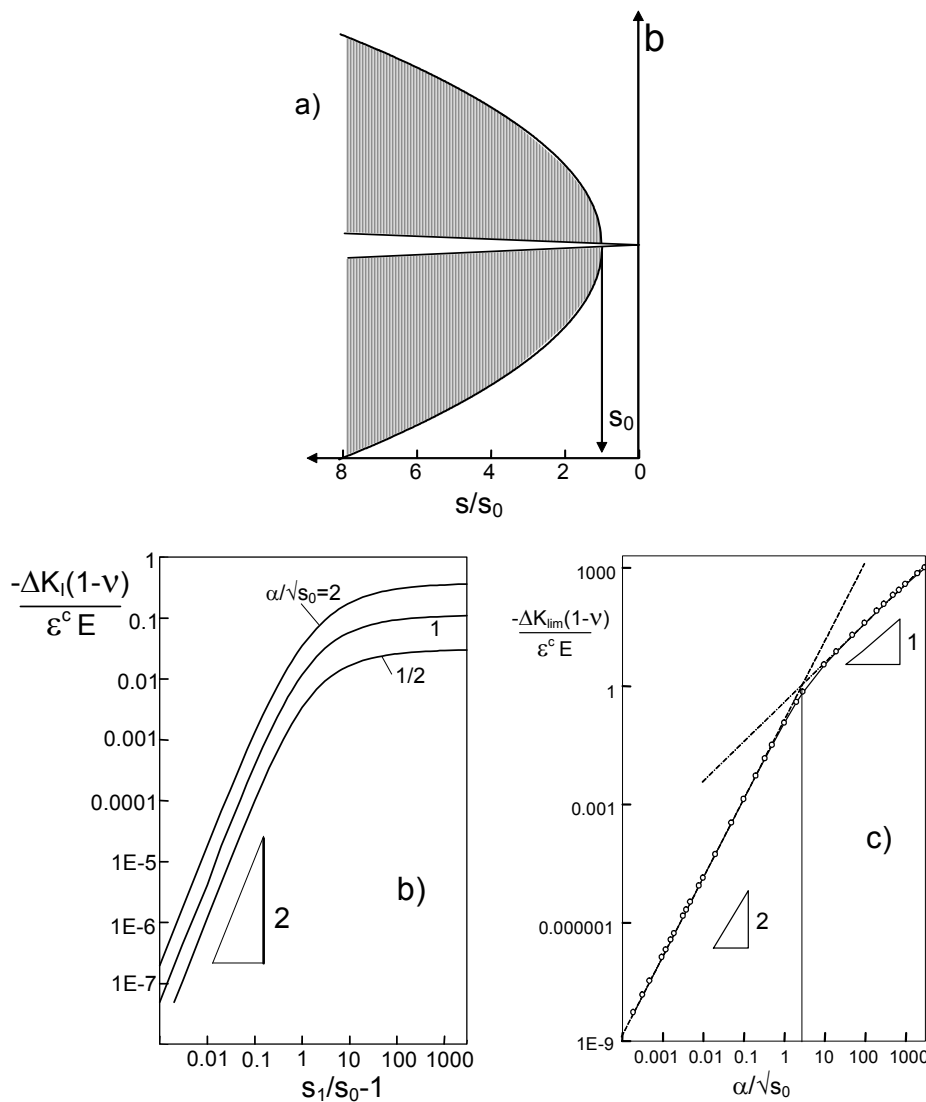


Fig. 13 a) Square-root-shaped zone profile ending at a distance $s_0 > 0$ from the crack tip, b) shielding stress intensity factor ΔK_I as a function of zone length s_1 , c) limit value ΔK_{lim} for varying values of α defined by eq.(30).

As can be seen from the intersection of the straight lines in Fig. 13b, the upper solution in eq.(40) is applicable for $\alpha/\sqrt{s_0} < 1$, the lower one for $\alpha/\sqrt{s_0} > 10$. A full interpolation is given by the approximation of

$$\Delta K_{\text{lim}} = -\frac{\varepsilon^c E}{1-\nu} \left[\left(\frac{2}{15} \alpha^2 / s_0 \right)^{-3/2} + \left(\frac{2}{5} \alpha / \sqrt{s_0} \right)^{-3/2} \right]^{-2/3} \quad (41)$$

The stress component σ_x at the crack surface ($y=0$) is shown in Fig. 14 for $s_0=0.1\alpha^2$. Maximum stresses are reached near $x=-s_0$.

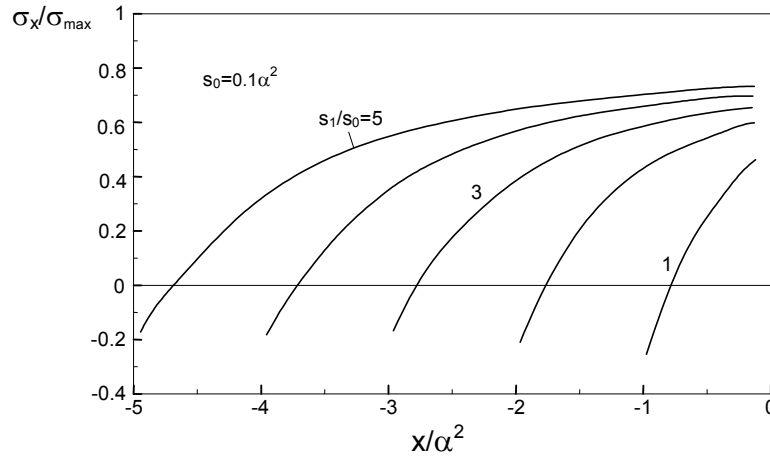


Fig. 14 Stress σ_x at the crack surface for a zone shape of Fig. 13a, several zone lengths, and $s_0=0.1\alpha^2$.

4.3 Superposition of solutions

A crack that has been loaded below the threshold for subcritical crack growth will exhibit a nearly constant zone thickness along the crack faces. If the applied stress intensity factor then is increased and exceeds the threshold, a square-root-shaped zone develops in the newly created crack region. The total zone shape is illustrated by Fig. 15. The stress intensity factor K_I and T-stress are obtained by superposition of the cases

$$b = \begin{cases} b_0 & \text{for } s > s_2 \\ b_1 \sqrt{s/s_2} & \text{for } s < s_2 \end{cases}, \quad b_0 > b_1 \quad (42)$$

with the stress intensity factor K_I resulting from eqs.(9) and (10) and the T-stress given by eqs.(24) and (26).

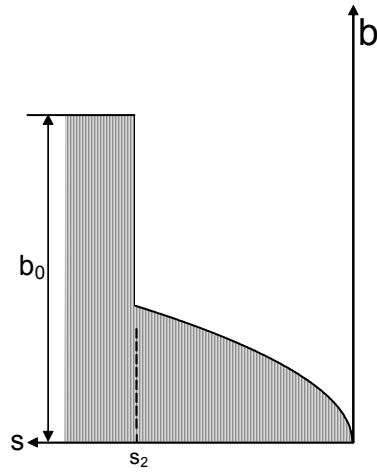


Fig. 15 Layer thickness profile of a crack loaded below the threshold for subcritical crack growth and additional crack extension after a load increase.

4.4 Strains varying with crack tip distance

In the case of a varying volumetric strain $\varepsilon^c=f(s)$, the strain has to be drawn under the integral. Then it holds for the mode-I stress intensity factor

$$\Delta K_I = \frac{E}{1-\nu} \int_0^{s_1} g_I(s'/b') \frac{\varepsilon^c(s')}{\sqrt{b'}} d(s') \quad (43)$$

References

- [1] McMeeking, R.M., Evans, A.G., Mechanics of transformation-toughening in brittle materials, *J. Am. Ceram. Soc.* **65**(1982), 242–246.
- [2] Budiansky, B., Hutchinson, J.W., Lambropoulos, J.C., Continuum theory of dilatant transformation toughening in ceramics, *Int. J. Solids Struct.* **19**(1983), 337–355.
- [3] Fett, T., Application of the weight function and boundary collocation method to the calculation of initial phase transformation zones, *Engng. Fract. Mech.* **52**(1995), 853-863.
- [4] Lucato, S.L., Lupascu, D.C., Rödel, J., Effect of poling direction on R-curve behavior in PZT, *J. Am. Ceram. Soc.* **83**(2000), 424-426.
- [5] Meschke, F., Raddatz, O., Kolleck, A., Schneider, G.A., R-curve behavior and crack-closure stresses in barium titanate and (Mg,Y)-PSZ ceramics, *J. Am. Ceram. Soc.* **83**(2000), 353-361.
- [6] Fett, T., Glazounov, A., Hoffmann, M.J., Munz, D., Thun, G., On the interpretation of different R-curves for soft PZT, *Engng. Fract. Mech.* **68**(2001) 1207-1218.
- [7] Glazounov, A., Fett, T., Reszat, J.T., Hoffmann, M.J., Munz, D., Wroblewski, T., Influence of domain switching state on R-curves interpreted by using X-ray diffraction study, *Journal of Materials Science Letters* **20** (2001), 877-880.
- [8] Michalske, T.A., Bunker, B.C., Keefer, K.D., Mechanical properties and adhesion of hydrated glass surface layers, *J. of Non-Crystalline Solids* **120**(1990), 126-137.
- [9] Michalske, T.A., Bunker, B.C., Effect of surface stress on stress corrosion of silicate glass, *Advances in Fracture Research*, **6**(1989), 3689-3701.
- [10] Bunker, B.C., Michalske, T.A., Effect of surface corrosion on glass fracture, *Fracture Mechanics of Ceramics*, Vol. 8 1986, 391-411, Plenum Press, New York.
- [11] Doremus, R.H., “Chemical Durability of Glass,” pp. 41 to 69 in “Treatise on Materials Science and Technology”, Vol. 17, Glass II, M. Tomozawa and R.H. Doremus, Eds. Academic Press, New York (1979).
- [12] Eshelby, J.D., Determination of the elastic field of an ellipsoidal inclusion and related problems, *Proc. R. Soc., London, Ser. A* **241**(1957), 376–396.
- [13] Tada, H., Paris, P.C., Irwin, G.R., *The stress analysis of cracks handbook*, Del Research Corporation, 1986.
- [14] Rice, J.R., Some remarks on elastic crack-tip stress fields, *Int. J. Solids and Structures* **8**(1972), 751-758.

APPENDIX

The near-tip displacement field for plane strain conditions reads [13]

$$u = \frac{K_{II}}{G} \sqrt{\frac{r}{2\pi}} \left(2 - 2\nu + \cos^2 \frac{\theta}{2} \right) \sin \frac{\theta}{2} \quad (\text{A1})$$

$$v = \frac{K_{II}}{G} \sqrt{\frac{r}{2\pi}} \left(-1 + 2\nu + \sin^2 \frac{\theta}{2} \right) \cos \frac{\theta}{2} \quad (\text{A2})$$

with
$$G = \frac{E}{2(1+\nu)} \quad (\text{A3})$$

The weight functions h_x and h_y can be obtained from the Rice equation [14] which relates the weight function to the change of displacement for a virtual crack extension ∂a under load K_{II} , i.e.

$$h_{II,x} = \frac{E'}{K_{II}} \frac{\partial u}{\partial a} \quad (\text{A4})$$

$$h_{II,y} = \frac{E'}{K_{II}} \frac{\partial v}{\partial a} \quad (\text{A5})$$

Evaluation of (A4) and (A5) then yields

$$h_{II,x} = \frac{1}{\sqrt{32\pi r(1-\nu)}} [4 - 4\nu + \cos(\theta) + \cos(2\theta)] \sin(\theta/2) \quad (\text{A6})$$

$$h_{II,y} = \frac{1}{\sqrt{32\pi r(1-\nu)}} [2 - 4\nu + \cos(\theta) - \cos(2\theta)] \cos(\theta/2) \quad (\text{A7})$$